Colloids and Surfaces B: Biointerfaces 210 (2022) 112260

Contents lists available at ScienceDirect

Colloids and Surfaces B: Biointerfaces

journal homepage: www.elsevier.com/locate/colsurfb

A gold nanoparticle-dye/poly(3-aminobenzylamine)/two dimensional $MoSe_2$/graphene oxide electrode towards label-free electrochemical biosensor for simultaneous dual-mode detection of cancer antigen 15-3 and microRNA-21

Chammari Pothipor [a,b,c], Suwussa Bamrungsap [d], Jaroon Jakmunee [a,c,e], Kontad Ounnunkad [a,c,e,f,*]

[a] Department of Chemistry, Faculty of Science, Chiang Mai University, Chiang Mai 50200, Thailand
[b] The Graduate School, Chiang Mai University, Chiang Mai 50200, Thailand
[c] Center of Excellence for Innovation in Chemistry, Faculty of Science, Chiang Mai University, Chiang Mai 50200, Thailand
[d] National Nanotechnology Center (NANOTEC), National Science and Technology Development Agency (NSTDA), Pathum Thani 12120, Thailand
[e] Research Center on Chemistry for Development of Health Promoting Products from Northern Resources, Chiang Mai University, Chiang Mai 50200, Thailand
[f] Center of Excellence in Materials Science and Technology, Chiang Mai University, Chiang Mai 50200, Thailand

ARTICLE INFO

Keywords:
Breast cancer biomarker
Label-free electrochemical biosensor
Simultaneous detection
Dual-mode biosensor

ABSTRACT

A dual-mode electrochemical biosensor is successfully developed for simultaneous detection of two different kinds of breast cancer biomarkers, namely cancer antigen 15-3 (CA 15-3) and microRNA-21 (miRNA-21), for the first time. The sensor composes of a poly(3-aminobenzylamine)/two-dimensional (2D) molybdenum selenide/graphene oxide nanocomposite modified two-screen-printed carbon electrode array (dual electrode), functionalized individually with 2,3-diaminophenazine-gold nanoparticles and toluidine blue-gold nanoparticles. Both kinds of the redox probe-gold nanoparticles are employed as signaling molecules and supports for immobilization of anti-CA 15-3 antibodies and capture DNA-21 probes, respectively. Due to the good conductivity and high surface-to-volume ratio of the nanocomposite, high amount of the antibodies and capture probes can be immobilized on the modified dual-electrode, giving the efficient duplex detection. Consequently, the biosensor provides good selectivity, and high sensitivity for the dual target analyte detection. The experimental results show that this label-free biosensor exhibits good linear responses to the concentrations of both target analytes with the limits of detection (LODs) of 0.14 U mL^{-1} and 1.2 fM for CA 15-3 and miRNA-21, respectively. This assay strategy has a great potential to be further developed for the simultaneous detection of a variety of miRNAs and protein biomarkers for point-of-care (POC) diagnostic applications.

1. Introduction

Breast cancer is one of the major causes of cancer-related death in woman worldwide [1,2]. The detection of breast cancer markers is significant for cancer screening, identifying the level of disease, and measuring response of the therapy [3,4]. Cancer biomarkers are biomolecules including secreted proteins, tumor-associated antigens, and nucleic acids (mutated DNA/RNA, mRNA, or microRNAs) [5,6]. These biomarkers are produced in the human body and their expression levels change during the tumor progression [7]. Due to the complexity of humoral immune responses in the human body, the assay of a single biomarker offers insufficient clinical information, which results in a poor prognosis [8]. Therefore, the development of highly sensitive, accurate, and multiplex biomarkers detection and profiling at the beginning of tumor promotion is required [9,10]. Recently, proteomic and genomic biomarkers have been employed to detect irregular gene expressions and mutations during cancer development [11]. Cancer antigen 15-3 (CA 15-3) is an acid glycoprotein with a high molecular weight of 300–450 kDa, which is found in patients suffered with a breast cancer [12,13]. Normally, the concentration of CA 15-3 in healthy human serum is typically less than 30 U mL^{-1}. If the serum level of CA 15-3 increases, high risk of breast cancer can be predicted [14]. Therefore,

* Corresponding author at: Department of Chemistry, Faculty of Science, Chiang Mai University, Chiang Mai 50200, Thailand.
E-mail address: kontad.ounnunkad@cmu.ac.th (K. Ounnunkad).

https://doi.org/10.1016/j.colsurfb.2021.112260
Received 26 September 2021; Received in revised form 25 November 2021; Accepted 2 December 2021
Available online 5 December 2021

the simple and sensitive detection and identification of CA 15-3 level in serum has become an important approach for breast cancer analysis. Besides the protein marker, microRNA (miRNA), a short-chain and endogenous nonprotein-coding RNA is another significant breast cancer marker related to gene expression [15] It has been reported that the level of miRNA-21 expression in breast cancer patients is much higher than that of the normal people [16]. The assay of both CA 15-3 and miRNA-21 is a promising candidate for efficient breast cancer diagnosis. Moreover, the early stage of breast cancer is confirmed by the over-expression level of such biomarkers [17]. Thus, the versatile, simultaneous analysis of the multiple biomarkers supports the accurate diagnosis and achievement of right treatment for patients [18,19]. This can be developed to point-of care (POC) diagnosing for many kinds of diseases and monitoring their treatments.

Many biosensors have been established for the simultaneous detection of multiple tumor markers with different signal transductions such as surface plasmon resonance [20], fluorescence [21], electrochemiluminescence [22], resonance light scattering [23], and electrochemical [24] techniques. Among them, electrochemical technique provides ease of operation including high specificity and sensitivity. Electrochemical sensors have shown several benefits, such as simultaneous detection, versatility, simple instrumentation, rapid detection, accurate quantification, low cost, good selectivity, and high sensitivity [25]. Previously, the biosensors for protein/RNA multi-analyte detection using both capture antibody and nucleic acid probe have been successfully developed [19,26,27]. However, the development of the stable, and rapid procedure toward label-free electrochemical technique is challenging. Electrochemical active species based on enzymes [28, 29], metal tags [30,31] or redox dyes [32,33] are commonly used as labels. Among these signaling particles/molecules, redox dyes such as anthraquinone, 2–3-diaminophenazine (DAP), methylene blue, toluidine blue (TB), and Prussian blue have attracted great interest due to their well-defined and strong voltammetric peaks at different potentials positions [34–38] that can be employed for signal molecules in multiplex immunosensor.

Interestingly, electrochemical biosensors' surfaces coated with the functional two-dimensional (2D) nanomaterials such as molybdenum diselenide ($MoSe_2$), molybdenum disulfide (MoS_2), tungsten diselenide (WSe_2), graphene, and graphene oxide (GO) have been reported with improved sensitivity for cancer analysis [38–43]. They provide high density of surface active sites resulting in increased detection sensitivity and making them ideal for construction of the devices [39]. The outstanding physiochemical properties of $MoSe_2$ such as fast charge transfer and large specific surface area, have made it a good choice for such sensing application [40]. Meanwhile, GO is another ideal material for the device fabrication due to its high surface area, high aqueous dispersibility and modification capability. Moreover, it is low cost, production scalability, ease of processing, and good biocompatibility [41,42]. Additionally, GO can react with various nanomaterials and conductive polymers or their derivatives to form novel nanocomposites [43,44]. It has been reported that the polyaniline derivatives can be used as electrochemical sensing matrices and improve stability of biomolecules immobilization on their surface [45–47]. Furthermore, gold nanoparticles (AuNPs) is frequently applied in this field because of their high conductivity and biocompatibility which can provide uniform electroactive sites, and large surface area for immobilization of biomolecules [48].

Herein, a novel dual electrochemical biosensor based on two different dye-AuNPs coated onto a poly(3-aminobenzylamine)/two-dimensional (2D) molybdenum selenide/graphene oxide (P3ABA/2D-$MoSe_2$/GO) nanocomposite modified two-working area screen-printed carbon electrode (2SPCE) array (dual electrode) for simultaneous determination of CA 15-3 protein and miRNA-21 has been developed. The nanocomposite on a 2SPCE array with a highly effective surface area is employed as the new platform, which allows deposition of DAP-AuNPs and TB-AuNPs for detection of CA 15-3 and miRNA-21, respectively. The sensing surface is further constructed via the immobilization of capture biomolecules, anti-CA 15-3 antibodies and DNA-21 capture probes, respectively, on the dual-electrode platform. The antibodies/DAP-AuNPs and DNA probes/TB-AuNPs sitting on each composite-modified working area of the platform are utilized as distinct signaling redox species to produce analytical responses. The CA 15-3 and miRNA-21 biomarkers are used as model analytes in the proposed proof-of-concept experiments. The present dual biosensor for the detection of both CA 15-3 and miRNA-21 shows wide ranges of linear responses, good multiplex ability, high sensitivity, high selectivity, acceptable reproducibility, and satisfied stability. This developed biosensor shows potential in accurate breast cancer diagnosis and can be further developed for the analysis or POC testing of other diseases.

2. Experimental section

2.1. Chemicals, reagents and apparatus

Chemicals and reagents, and apparatus are listed in Sections S1 and S2 (Supporting information), respectively.

2.2. Preparation of nanomaterials

Graphene oxide was prepared from graphite powder according to the modified Hummer's method [49]. The preparation of 2D-$MoSe_2$ was according to the modified procedure of the literature [50]. A portion of 0.5 g of bulk $MoSe_2$ powder was added into 0.4 mL of N-methyl-2--pyrrolidone. The mixture was ground in an agate mortar for 1 h. To remove the solvent, the resultant viscous mixture was dried in an oven at 60 °C overnight. The 2D-$MoSe_2$ powders were obtained. To make the 2D nanocomposite, the graphene oxide and 2D-$MoSe_2$ powders at 4.0 mg mL^{-1} were dispersed separately in deionized water and mixture of isopropanol: deionized water (90:10 v/v), respectively under sonication for 1 h. The graphene oxide dispersion was mixed with the $MoSe_2$ nanosheet dispersion in a sonicator for 1 h and kept with a total concentration of 4.0 mg mL^{-1}. The graphene oxide/2D-$MoSe_2$ composite dispersion was used to further fabricate a signaling nanocomposite-coated 2SPCE array. Two kinds of dye-AuNPs were prepared by mixing 180 μL of 10% w/v $HAuCl_4$ solution and 20 μL of 100 mM TB or DAP in 0.010 M PBS (pH 7.4) on thermomixer at 400 rpm and at the temperature of 25 °C for 4 h [24]. The resulting composites were separated and washed with deionized water by centrifugation at 7000 rpm for 3 times. For future use, each nanocomposite was re-dispersed and adjusted with deionized water to a 200-μL volume. The morphologies of the nanomaterials are described in Section S5 (Supporting information).

2.3. Preparation of modified electrodes

The procedure for electrode modification and electrochemical measurements are described in Sections S3 and S4 (Supporting information), respectively. The morphological properties of the modified electrodes are also described in Section S5 (Supporting information).

2.4. Construction of dual immunosensor-DNA bioplatform

Our dual biosensor is divided into two parts involving immunosensor and DNA-based biosensor. The simultaneous detection of CA 15-3 protein and miRNA-21 is achieved by monitoring both immunoreaction and hybridization, respectively. The fabrication and optimization of the sensor and its multiplex detection were evaluated at room temperature. The principle of proposed dual biosensor is demonstrated in Fig. S3. For the detection of CA 15-3 protein, 2.5 μL of DAP-AuNPs solution was dropped on the first nanocomposite-modified working SPCE of an array and then dried in air at the room temperature. For the activation of terminal carboxylic groups of anti-CA 15-3 antibodies, 50 μL of 0.40 M EDC/0.10 M NHS (1:1 v/v) solution and 50 μL of 60 μg mL^{-1} anti-CA 15-

3 solution were mixed on thermomixer at 400 rpm [51]. 2.5 μL of activated anti-CA 15-3 antibodies solution was incubated onto the modified electrode in a humidity chamber for 1 h. The unbound anti CA 15-3 antibodies were removed from the modified electrode by rinsing with 10 mM PBS (pH 7.4) for 3 times. To avoid non-specific adsorption of proteins, free surface sites of the electrode were blocked with 2.5 μL of 0.5% w/v BSA solution for 30 min and the electrode was washed with PBS solution for 3 times. For the measurement of miRNA-21, the capture DNA-21 solution was prepared by mixing 10 μL of 0.2 mM TCEP-HCl in 10 mM Tris EDTA solution and 10 μL of 20 μM capture DNA-21 at 400 rpm for 2 h to break S-S bond. 2.5 μL of TB-AuNPs was dropped on to the second nanocomposite-modified working SPCE and then left in the air at room temperature. Furthermore, 2.5 μL of the capture DNA-21 solution was immobilized onto the resultant modified SPCE in the humidity chamber for 2 h. After the incubation of capture DNA-21, the capture DNA-21/TB-AuNPs/nanocomposite-modified SPCE was gently rinsed with 1 ×PBS to remove unbound capture DNA-21 probes for 3 times. 2.5 μL of 20 μM MCH blocking solution was coated on to the nanocomposite-modified SPCE containing the capture DNA 21 and TB-AuNPs for 30 min and then washed with PBS for 3 times. The stock target miRNA-21 solution was prepared in hybridization buffer (1 × SSC) solution. For the simultaneous detection of both CA 15-3 and miRNA-21, the quantitation was carried out using 2.5 μL droplets of target CA 15-3 and miRNA-21 solutions in the immunoreaction and hybridization on the first and second electrodes, respectively for 1 h. Consequently, the both array electrodes were rinsed with PBS several times to remove unbound miRNA-21 and CA 15-3, followed by electrochemical measurement. The electrochemical responses of two redox dyes before and after immobilization of target protein and miRNA were recorded by DPV technique in 0.01 M PBS buffer (pH 7.4).

3. Results and discussion

3.1. Electrochemical properties of nanocomposite-modified electrodes

As compared to the electrochemical properties of the bare SPCE, Fig. 1a shows that the CVs of the electrodes modified with different materials are evaluated in 0.10 M KCl solution containing 5 mM $[Fe(CN)_6]^{4-/3-}$ at a scan rate of 50 mV s^{-1}. All electrodes reveal a pair of well-defined redox peaks of $[Fe(CN)_6]^{4-/3-}$ (Fig. 1a). Peak currents slightly increase by coating SPCE with 2D-$MoSe_2$ nanosheets, which indicates the inherent conductive behaviour of selenium in 2D-$MoSe_2$ structure (Fig. 1a-blue curve) [40]. After the graphene oxide is covered on SPCE, the peak current response increases compared to that of the bare SPCE (Fig. 1a-red curve). This results from the high reactivity of high quality graphene oxide, which the electrode-surface modification with graphene oxide can increase current response and encourage the quicker electron transfer process [52–54]. After the SPCE and graphene oxide-modified SPCE are modified with P3ABA, the peak currents increase, indicating that the P3ABA film is successfully deposited onto both SPCEs (Fig. 1a-pink and green curves). This conducting polymer derivative improves the electrochemical reactivity and compatibility at the electrode/electrolyte interface, resulting in faster electron transfer kinetics and electrochemical response. In the same way, the highest peak current is observed after the P3ABA is deposited on graphene oxide/2D-$MoSe_2$-modified SPCE (Fig. 1a-orange curve). The EIS spectra of the modified electrodes in contact with 0.10 M KCl containing 5.0 mM $[Fe(CN)_6]^{4-/3-}$ are shown in Fig. 1b. The semicircles at high-frequency region correspond to resistances of the charge transfer (R_{ct}). Generally, the R_{ct} value is an important factor reflecting the interface properties of the modified electrodes' surfaces. The R_{ct} value of the bare SPCE is 101 Ω. After the P3ABA, 2D-$MoSe_2$, graphene oxide, P3ABA/graphene oxide and P3ABA/2D-$MoSe_2$/graphene oxide films are covered on the SPCEs, it decreases to *ca.* 89, 78, 60, 58, 54 Ω, respectively, due to the good nanomaterials' conductivity. The nanomaterials offers better charge transfer process at the electrolyte/electrode interface. The modification of electrode surface leads to a decrease in R_{ct} value that in turn governs the electrode kinetics. It is probably attributed to topological features of the electrode surface after the modification, which causes the fractal dimension of porous or rough surfaces-electrodes [55]. The surface morphological characters of the modified electrodes would result in lowered and/or distorted semicircle and the depression of the semicircle center in the EIS spectra due to the capacitance dispersion [55–57]. EIS result agrees well with those of the CV measurement, signifying successful preparation of the three-component nanocomposite-modified 2SPCE array. The electrode array with the best conductive properties would be served for further modification with dye-AuNPs and biomolecules (anti-CA 15-3 and DNA-21 capture probe) for fabricating a novel, label-free, highly sensitive, and duplex biosensor.

3.2. Construction of the dual biosensor

Since a 2SPCE array is employed to construct the proposed label-free immuno- and DNA-based biosensor, they are connected via the array structure for detection of CA 15-3 protein and miRNA-21 biomarkers within a single run. Fig. 2 demonstrates the fabrication of the sensing surfaces and the corresponding DPV curves of the modified electrodes with different modification steps, measured in contact with 10 mM PBS (pH 7.4). For a nanocomposite-modified 2SPCE array without deposited redox dye species-AuNPs (DAP-AuNPs and TB-AuNPs), no obvious peak

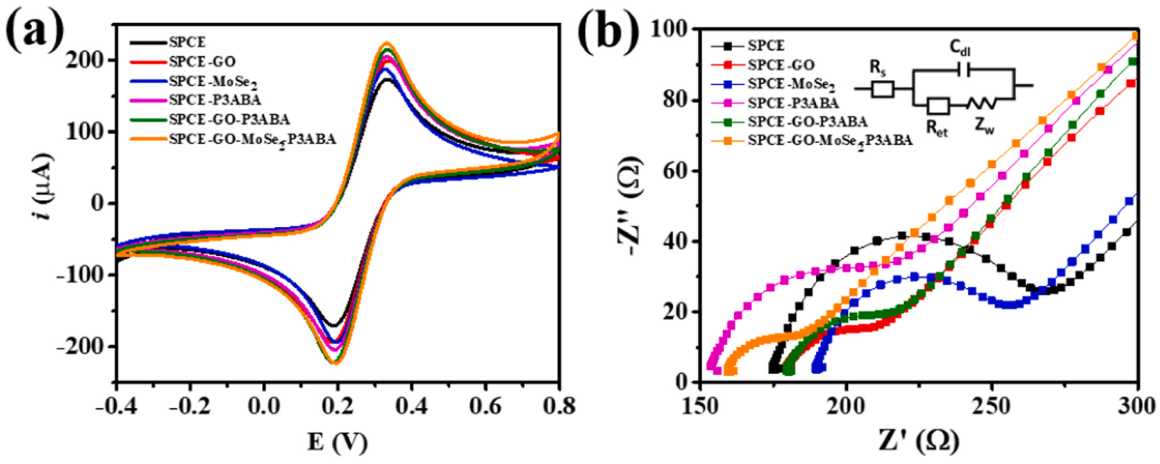

Fig. 1. (a) CVs curve and (b) Nyquist plots of bare SPCE and GO-, 2D-$MoSe_2$-, P3ABA-, P3ABA/GO-, and P3ABA/2D-$MoSe_2$/GO-modified SPCEs in contact with 0.10 M KCl solution containing 5 mM $[Fe(CN)_6]^{3-/4-}$.

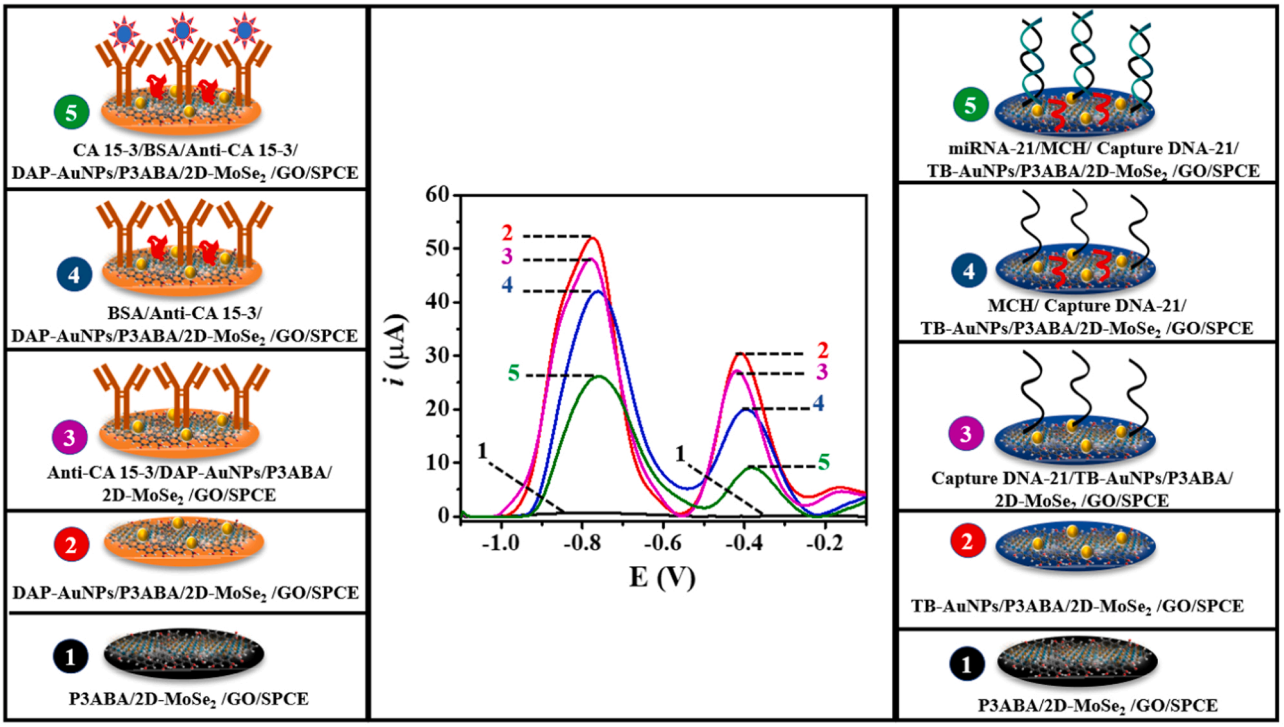

Fig. 2. DPVs of (1) bare nanocomposite-modified 2SPCE array and (2) dyes-AuNPs-, (3) anti-CA 15-3/ and capture DNA-21 probe/dyes-AuNPs-, (4) BSA/anti-CA 15-3/ and MCH/capture DNA-21 probe/dyes-AuNPs-, and (5) CA 15-3/BSA/anti-CA 15-3/ and miRNA-21/MCH/capture DNA-21 probe/dyes-AuNPs-coated nanocomposite-modified 2SPCE arrays in 10 mM PBS solution (pH 7.4).

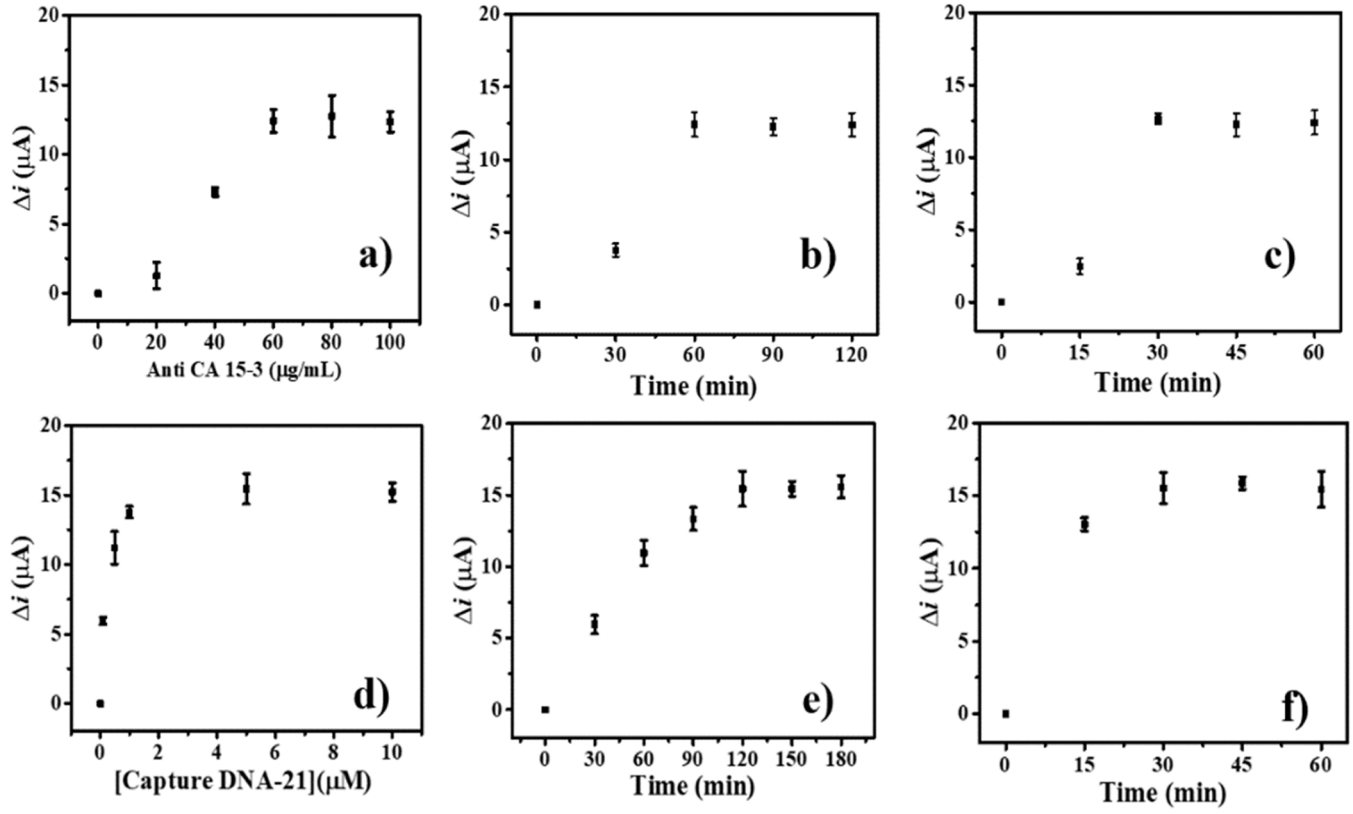

Fig. 3. Influences of (a, d) anti-CA 15-3 and capture DNA-21 probe concentrations, (b, e) anti-CA 15-3 and capture DNA-21 anchoring time, and (c, f) the immunoreaction/hybridization time on responses for the simultaneous detection of CA 15-3 and miRNA-21 using the developed biosensor.

is observed (curve 1). After DAP-AuNPs and TB-AuNPs are coated on the nanocomposite-modified 2SPCE array, distinct anodic current peaks of DAP and TB located at − 0.80 V and 0.4 V, respectively, are observed (curve 2). This indicates that the nanocomposite is a good electrochemically reactive support for DAP and TB of the AuNPs-based nanocomposites and performs well-defined redox processes. After immobilization of anti-CA 15-3 antibodies and DNA-21 capture probes onto DAP-based and TB-based nanocomposites of the modified 2SPCE array, respectively, the peak currents of DAP and TB decrease (curve 3) because the electrode-assembled anti-CA 15-3 antibodies and DNA-21 probes hinder their electron transfer processes at each SPCE of the array. Then, to get rid of the left non-specific adsorption/surface active sites, both current peaks further decline after BSA and MCH blocking agents are attached on the nanocomposite-modified SPCEs coated with anti-CA 15-3/DAP-AuNPs and DNA-21/TB-AuNPs, respectively (curve 4). After the target CA 15-3 and miRNA-21 are captured with their corresponding probes, significant decreases in both DPV peaks are observed (curve 5). This is attributed to the specific target-probe binding and target miRNA-probe hybridization which also hinder electron transfer processes of both dyes.

3.3. Optimization of device fabrication conditions

In this study, the dual immunosensor-DNA biosensor device is developed using the modified array consisting of two working electrodes for simultaneous and individual electrochemical detection of CA 15-3 and miRNA-21. To obtain the best sensor, the optimization of fabrication conditions is required. The amount of the immobilized anti-CA 15-3 and capture DNA-21 probes on the surfaces of the developed nanocomposite-modified SPCE-based dual biosensor is one of the key factors affecting detection sensitivities of the target analytes. Moreover, the experimental parameters including antibodies' and DNA probes' anchoring time, and detection time of both protein CA 15-3 and miRNA-21 were also investigated to achieve the best biosensing efficiency. Fig. 3a and d show effect of the antibody and DNA probe concentrations on the device performance. After incubation of the redox dyes-AuNPs/nanocomposite-modified 2SPCE array with the capture antibody (anti-CA 15-3) and DNA probe (DNA-21) solutions, the electrodes were washed with PBS many times and used in the optimization via the multiplex detection of CA 15-3 and miRNA-21. The concentrations of anti-CA 15-3 and DNA-21 were varied from 20 to 100 μg mL^{-1} and from 0.10 to 10 μM with the incubation times for the probes immobilization of 1 and 2 h, respectively, while the immunoreaction/hybridization time for this optimization is 1 h. Consequently, the detection was performed simultaneously. In general, decreases in the responses due to the numbers of target CA 15-3 and miRNA-21 captured on a nanocomposite-modified 2SPCE array, are dependent on the anti-CA 15-3 and DNA-21 probe contents. If the amounts of surface-bound probes are higher, the amounts of both captured target analytes are higher, causing the larger current differences before and after targets' binding. As displayed in Fig. 3a, 100 U mL^{-1} CA 15-3 is detected by the dual biosensor using anti-CA 15-3 with the concentrations from 20 to 100 μg mL^{-1}. The change in peak current (Δi) increases with raising the anti-CA 15-3 concentration from 20 to 60 μg mL^{-1} and then reaches the constant level (*ca.* 12.4 μA) from the concentration of 60 μg mL^{-1} onward, indicating the saturated immobilization of anti-CA 15-3 antibodies. Therefore, the optimal anti-CA 15-3 concentration of 60 μg mL^{-1} is selected for the fabrication of the immunosensor. To optimize the concentration of the DNA-21 capture probe for electrode-surface immobilization via detection of the hybridization reaction of miRNA-21/DNA-21 duplex, the biosensors employing a gradient of DNA-21 probe concentrations are constructed. As shown in Fig. 3d, by increasing the concentration of the DNA-21 probe from 0.10 to 10 μM, the detection of 10 pM miRNA-21 by the fabricated biosensor is tested. It is found that the Δi value increases up to 5 μM (*ca.* 15.3 μA), and then no significant change is observed because of saturation of DNA-21 probe molecules on the electrode surface. At the saturation point, dual biosensor does not capture more targets due to the same quantities of probes immobilized on the both array SPCE surfaces. Therefore, at high probe concentrations, the current does not change significantly. The DNA-21 probe concentration of 5 μM is selected to fabricate another part of the dual biosensor.

With keeping the constant concentrations of the antibodies and DNA probe at the optimized values and the immunoreaction/hybridization time of 1 h, the effect of incubation times for the immobilization of the anti-CA 15-3 and DNA-21 on the sensor sensitivities was studied. Time range from 30 to 120 min for immobilization of the activated antibodies is demonstrated in Fig. 3b. The Δi value of the detection of 100 U mL^{-1} CA 15-3 increases quickly with extending incubation time to 60 min and then reaches a plateau, thus implying a saturated binding between the antigen and the antibody on electrode surface due to limited binding sites of the electrode surface or limited amounts of the antibody. This means that after 60 min, the immobilization of antibody is complete and the anti-CA 15-3 antibody cannot further bind. So, 60 min is the optimal time for the immobilization of anti-CA 15-3. Furthermore, the DNA-21-immobilization time from 30 to 100 min is studied as shown in Fig. 3e. According to this figure, the time for complete hybridization between DNA-21 capture probe and miRNA-21 target is still kept at 1 h. The Δi value from binding with 10 pM miRNA-21 increases with increasing the immobilization/incubation time until 120 min and it thereafter is constant indicating that at this point, the electrode surface is full decorated by the DNA-21 capture probes. This incubation time cause completion of DNA-21 capture probes attachment on the sensing surface. In comparison with anti-CA 15-3 anchoring time, the time required for immobilization of capture DNA-21 probe is longer since the antibody is activated whilst DNA-21 capture probe is attached via automatically formed S-Au bonds. Therefore, the optimized immobilization time of 120 min is used throughout the whole sensing experiment.

Additionally, the incubation times for the CA 15-3/anti-CA 15-3 immunoreaction and miRNA-21/DNA-21 hybridization are critical factors to affect the devices' quality. The constant Δi values indicate the complete immunoreaction/hybridization. As observed in Fig. 3c, the time was varied from 15 to 60 min for the determination of 100 U mL^{-1} CA 15-3 by our developed biosensor. It is found that the Δi response increases up to the 30 min. After that, the current response does not change due to the saturated capturing of CA 15-3 on the electrode surface. Thus, 30 min is chosen for the sensing of CA 15-3. Moreover, various hybridization times, including 15, 30, 60, and 120 min were used for detection of 10 pM miRNA-21 by the dual biosensor. The hybridization time of target miRNA-21 is evaluated in Fig. 3f. The Δi value reaches the maximum when the hybridization time exceeds 30 min, and then remains constant. Consequently, the incubation time of 30 min is applied for miRNA-21 detection.

3.4. Multiplex capability of the dual biosensor

The multiplex capability of this electrochemical biosensor was investigated by the single-run detection of both CA 15-3 and miRNA-21 employing our dual biosensor. The simultaneous detection were controlled under the optimized experimental conditions. The recognition of each array SPCE in contact with solutions in the presence and/or absence of protein CA 15-3 and/or miRNA-21, was studied by differential pulse voltammetry (DPV). Without both target analytes, two baseline current peaks of the fabricated dual biosensor, located at the applied potentials of − 0.78 V and 0.40 V, are observed (Fig. 4a–c, black line). After the dual sensor is soaked with the solution containing both 100 U mL^{-1} CA 15-3 and 10 pM miRNA-21, both DPV current peaks considerably decrease as can be seen in Fig. 4a (red line). After incubation with the solution containing 100 U mL^{-1} CA 15-3 without miRNA-21, a reduced DPV peak at the potential of − 0.78 V was observed and the peak height at the potential of 0.40 V does not change significantly (Fig. 4b, red line). On the other hand, only DPV current

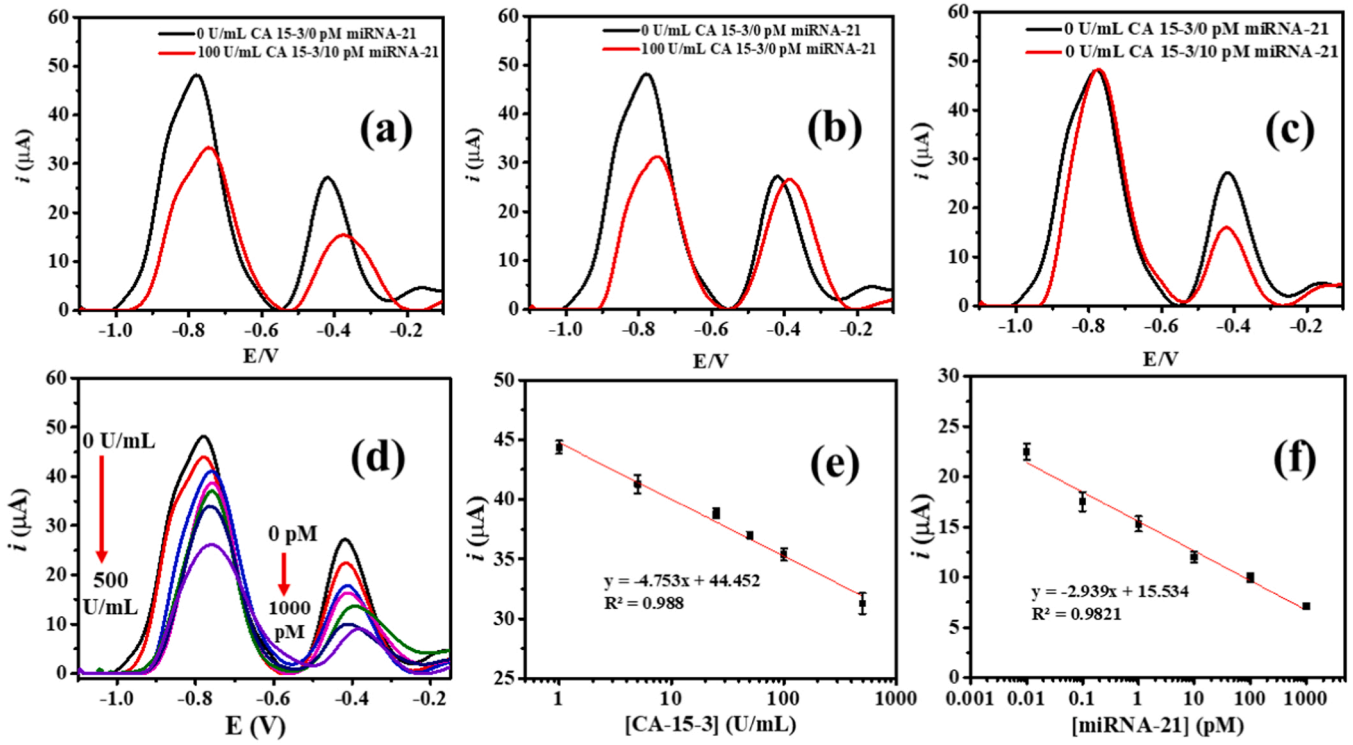

Fig. 4. Cross-reactivity investigation of the electrochemical dual biosensor by simultaneous detection of both targets. The measured DPV responses of DAP and TB confined on the dual biosensor with presence of 0 U mL^{-1} CA 15-3 + 0 pM miRNA-21 (black), and (a) 100 U mL^{-1} CA 15-3 + 10 pM miRNA-21 (red), (b) 100 U mL^{-1} CA 15-3 + 0 pM miRNA-21 (red), and (c) 0 U mL^{-1} CA 15-3 + 10 pM miRNA-21 (red). (d) DPV responses of the proposed biosensor after incubation with different concentrations of CA 15-3 and miRNA-21 and corresponding calibration curves of the duplex assay toward CA 15-3 (e) and miRNA-21 (f) in 0.10 M PBS solution (pH 7.4).

peak at the potential of 0.40 V declined obviously when the sensor is immersed in 10 pM miRNA-21 solution at the absence of CA 15-3 (Fig. 4c, red line). In Fig. 4a and b, the peak heights at the position of − 0.78 V are identical when immunoreaction occurs with 100 U mL^{-1} CA 15-3, whilst in Fig. 4c, the peak height at the potential of 0.40 V is insignificantly different from that in Fig. 4a due to similar hybridization of miRNA-21 and DNA-21. This confirms that each sensing element on each SPCE of the dual biosensor recognizes their own corresponding targets with no cross binding and non-specific adsorption. It is plausible that the cross reactivity between two target analytes or current additivity to each other is negligible. Therefore, the simultaneous multi-analyte bioassay with high precision and accuracy can be achieved by the proposed dual biosensor.

3.5. Analytical performance of the dual biosensor

To evaluate the device analytical performance, under the optimized condition, the DPV curves of the dual biosensor after specifically and simultaneously capturing CA 15-3 and miRNA-21 at various concentrations of 0–500 U mL^{-1} and 0–1000 pM, respectively, are measured at room temperature (Fig. 4d). The decreases in DPV response peaks for the multiplex detection are observed, which are proportional to the amount of target biomarkers. It is noted that amounts of insulating layers formed together with immunocomplexes and hybridization products (miRNA-21/DNA-21 duplexes) increase with increasing the target concentrations. Thus, electron transfer blockage of both dyes is raised, resulting the reduced current responses. Correspondingly, Fig. 4e demonstrates the great linearity between the current response and the logarithm of the CA 15-3 antigen concentration, and Fig. 4f also reveals the good linear relationship between the current intensity and the logarithm of the concentrations of the miRNA target. The limits of quantification (LOQs) and the limits of detection (LODs) are evaluated from the calibration plots using the equations; LOQ is $10SD_{blank}/m$ and LOD is $3SD_{blank}/m$, where SD_{blank} is the standard deviation of the blank and m is the slope of the calibration plot [58,59]. It is found that the calculated LOQs are 0.47 U mL^{-1} and 4.1 fM for the detections of CA 15-3 and miRNA-21, respectively. In case of CA 15-3 detection, the LOD is found to be 0.14 U mL^{-1} while the LOD of miRNA-21 is 1.2 fM. When considering the cut-off level of CA 15-3 (25 U mL^{-1}) in the clinical evaluation, the LOQ is sufficient for quantification of this biomarker. Thus, the fabricated dual biosensor is beneficial in the breast cancer diagnostics.

3.6. Selectivity, reproducibility and stability of the dual biosensor

To evaluate the specificity of the dual biosensor, the simultaneous detection of both targets is carried out to obtain the current responses regarding all the solutions. Interfering substances such as AFP, IgG, GM2, Glu, AA, UA, and BSA are selected as the interferences to evaluate the selectivity of the immunosensor. As shown Fig. 5a, the selectivity of the biosensor is tested using 25 U mL^{-1} CA 15-3 target protein and PBS is used as the blank. The interference study for immunosensor part is divided into two groups. The first group involves individual interferences (100 ng mL^{-1}) without the presence of the target protein. The second group involves the incubation of the sensing surface with 25 U mL^{-1} CA 15-3 solutions containing individual interfering substances or their mixture (100 ng mL^{-1}). The current responses of the first group are slightly different from that of the blank (PBS) with the current variation less than *ca.* 3.3%. The response values of the second group does not significantly change as compared to that of the solution containing only CA 15-3. Moreover, the variation of analytical response produced by the interference substances contained in the matrix together with the target biomarker of interest is less than *ca.* 1.0%. Although individual interference causes higher variation of baseline response, in practical use the detection employs the analytical response

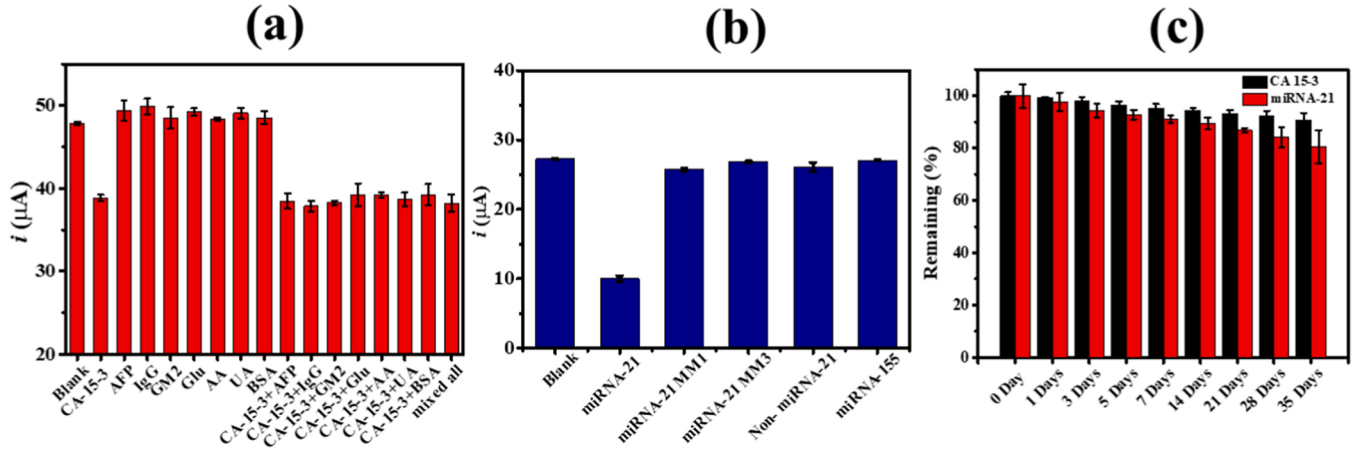

Fig. 5. (a) responses of the anti-CA 15-3 immobilized DAP-AuNPs/nanocomposite-modified SPCE toward the detection of blank, 100 U mL^{-1} CA 15-3, 100 ng mL^{-1} individual interferences (AFP, IgG, GM2, Glu, AA, UA, and BSA), 100 U mL^{-1} CA 15-3+ each interference (100 ng mL^{-1}), and 100 U mL^{-1} CA 15-3+ all interference mixture (100 ng mL^{-1} each), (b) responses of the DNA probe immobilized TB-AuNPs/nanocomposite-modified SPCE toward the detection of blank solution, 100 pM miRNA-21, and 100 pM individual oligonucleotide interferences (single base mismatched target (MM1), triple bases mismatched target (MM3), non-complementary miRNA-21, and miRNA-155), and (c) stability test of the biosensor over 5 weeks for duplex detection of CA 15-3 and miRNA-21.

from the detection in the real matrix containing many kinds of interfering biological substances together with the target biomarker of interest. The matrix also contain many biological substances. It is noted that the presence of interferences does not provide different responses in the detection of CA 15-3 compared to that of the detection without interference, suggesting the satisfied specificity of the immunosensor to CA 15-3. In the case of miRNA-21 biosensor part, single-base mismatch (1MM), triple-base mismatch (3MM), and non-complementary miRNAs, and miRNA-155 are used as interferences as depicted Fig. 5b. The selectivity test of the biosensor is performed by the detection of all single miRNA (100 pM) solutions. Again, the reduced response is exactly observed when the sensor is incubated with 100 pM miRNA-21 solution due to the miRNA-21/ DNA-21 capture probe hybridization. As compared to the blank response, no significant change in the response is observed from the detection of 1MM, 3MM, non-complementary miRNAs, and miRNA-155, indicating no formation of hybridization product. This implies that the prepared sensor exceedingly possesses high specificity for miRNA-21.

In addition, to investigate the reproducibility of the dual biosensor, the detection of both analytes by five individual biosensing 2SPCE arrays are tested under the same condition. The concentrations of the target analytes, CA-153 and miRNA-21, are 1.0 U mL^{-1} and 0.1 pM, respectively (Fig. S8). Relative standard deviations (%RSD) of the analytical responses after binding with the same concentrations of CA 15-3 and miRNA-21 are 4.15% and 4.87%, respectively, favoring the good reproducibility and precision of the dual biosensor. Moreover, to test the device stability, the prepared dual biosensors are kept at 4 °C over a period of time from 1 day to 35 days (five weeks) and the multiplex detection of both analytes is performed for each storage time. The analytical responses change over the time as shown in Fig. 5c. The response of the CA 15-3 detection (100 U mL^{-1}) after 5 weeks retains *ca.* 91% of its initial value. In addition, *ca.* 81% of the initial response for detection of miRNA-21 (100 pM) is found when the sensor is stored for 5 weeks. Thus, the performance of this proposed dual biosensor is sufficient for detection of the biological objectives of interest. The knowledge from this study can be extended in the development of other multiplexed assays. The developed device meets the requirement of the simultaneous detection strategy.

3.7. Simultaneous detection by the dual biosensor

For the applicability of the proposed biosensor, a human serum sample is selected as the biological sample. The serum sample was 50% diluted with 0.01 M PBS for recovery study [60]. Subsequently, the CA 15-3 and miRNA-21 solutions with three concentrations (5.0, 50, and 100 U mL^{-1} for CA 15-3, and 1.0, 10, and 100 pM for miRNA-21) are freshly prepared into the diluted human serum. The dual biosensor is applied to analyze CA 15-3 and miRNA-21 simultaneously in the prepared solutions. Table 1 shows the result of recovery test for the detection. The percentages of recovery (% recoveries) are in the range of 100.5–109.9% with the %RSD range of 1.13–2.82% for CA 15-3 detection. For the miRNA-21 determination, the % recoveries are 104.5–110.0% with %RSD values of 4.13–6.26%. Therefore, the proposed nanocomposite-modified 2SPCE biosensor exhibits acceptable recoveries for the duplex detection of CA 15-3 protein and miRNA-21 in human serum, which is feasible for clinically analytical applications in the future.

4. Conclusions

A label-free dual electrochemical biosensor using the newly designed three-component nanocomposite-modified 2SPCE array is successfully developed for the simultaneous detection of cancer-associated CA 15-3 and miRNA-21. The nanocomposite improves the electron transfer kinetics. The two redox dye/AuNPs composites are used as the signal generators for the detection of both CA 15-3 and miRNA-21. The prepared DAP-AuNPs- and TB-AuNPs-based nanocomposites possess favorable bioactivity and act as a support the immobilization of anti-CA 15-3 antibody and DNA-21 capture probe, respectively. Under the optimal condition, the proposed assay strategy reveals excellent analytical performance, and the biosensor can perform the analysis at the femtomolar level (1.2 fM) for miRNA-21 and with the LOD of 0.14 U mL^{-1} for CA 15-3. The developed biosensor provides not only fast analytical response time but also simplicity in preparation, high selectivity, reproducibility, and acceptable stability. Thus, this biosensor is a useful tool for the early stage breast cancer detection. In addition, the approach has provided a new avenue for multiplex sensing applications and held great promise for disease diagnostic with a potential in developing POC diagnostic devices.

CRediT authorship contribution statement

Chammari Pothipor: Investigation, Results analysis. **Jaroon Jakmunee:** Writing – review & editing. **Suwussa Bamrungsap:** Writing – review & editing. **Kontad Ounnunkad:** Conceptualization, Methodology, Validation, Resources, Writing – original draft, Writing – review &

Table 1
Recovery result obtained from the proposed CA 15-3 and miRNA-21 biosensor in serum sample.

Samples	CA 15-3				miRNA-21			
	Added [U mL^{-1}]	Detected [U mL^{-1}]	Recovery [%]	RSD [%]	Added [pM]	detected [pM]	Recovery [%]	RSD [%]
1	5.0	5.18 ± 0.06	103.6	1.13	1.0	1.05 ± 0.04	104.8	4.13
2	50.0	50.26 ± 1.42	100.5	2.82	10.0	10.99 ± 0.57	110.0	4.25
3	100.0	109.89 ± 2.71	109.9	2.46	100.0	104.51 ± 6.54	104.5	6.26

editing, Visualization, Supervision, Project administration, Funding acquisition.

Declaration of Competing Interest

The authors declare that they have no known competing financial interests or personal relationships that could have appeared to influence the work reported in this paper.

Acknowledgements

C.P. would like to thank an award of the Thailand Graduate Institute of Science and Technology (TGIST) 2017 (Grant No. TG-55-10-60-025D), National Science and Technology Development Agency (NSTDA), Thailand. This research work was partially supported by Chiang Mai University (CMU). K.O. would like to thank the Research Center on Chemistry for Development of Health Promoting Products from Northern Resources, the Center of Excellence for Innovation in Chemistry (PERCH-CIC), and Faculty of Science (CMU).

Appendix A. Supporting information

Supplementary data associated with this article can be found in the online version at doi:10.1016/j.colsurfb.2021.112260.

References

[1] S.M. McKinney, M. Sieniek, V. Godbole, J. Godwin, N. Antropova, H. Ashrafian, T. Back, M. Chesus, G.S. Corrado, A. Darzi, M. Etemadi, F. Garcia-Vicente, F. J. Gilbert, M. Halling-Brown, D. Hassabis, S. Jansen, A. Karthikesalingam, C. J. Kelly, D. King, J.R. Ledsam, D. Melnick, H. Mostofi, L. Peng, J.J. Reicher, B. Romera-Paredes, R. Sidebottom, M. Suleyman, D. Tse, K.C. Young, J. De Fauw, S. Shetty, International evaluation of an AI system for breast cancer screening, Nature 577 (2020) 89–94.
[2] E. Vargas, E. Povedano, V.R.V. Montiel, R.M. Torrente-Rodríguez, M. Zouari, J. J. Montoya, N. Raouafi, S. Campuzano, J.M. Pingarrón, Single-step incubation determination of miRNAs in cancer cells using an amperometric biosensor based on competitive hybridization onto magnetic beads, Sensors 18 (2018) 863.
[3] L.L. Wang, Early diagnosis of breast cancer, Sensors 17 (2017) 1572.
[4] L. Wu, X. Qu, Cancer biomarker detection: recent achievements and challenges, Chem. Soc. Rev. 44 (2015) 2963–2997.
[5] M. Mohammadniaei, H.V. Nguyen, M.V. Tieu, M.H. Lee, 2D materials in development of electrochemical point-of-care cancer screening devices, Micromachines 10 (2019) 662.
[6] B.S. Munge, T. Stracensky, K. Gamez, D. DiBiase, J.F. Rusling, Multiplex immunosensor arrays for electrochemical detection of cancer biomarker proteins, Electroanalysis 28 (2016) 2644–2658.
[7] S. Rapisuwon, E.E. Vietsch, A. Wellstein, Circulating biomarkers to monitor cancer progression and treatment, Comput. Struct. Biotechnol. J. 14 (2016) 211–222.
[8] F. Wei, P. Patel, W. Liao, K. Chaudhry, L. Zhang, M. Arellano-Garcia, S. Hu, D. Elashoff, H. Zhou, S. Shukla, F. Shah, C.M. Ho, D.T. Wong, Electrochemical sensor for multiplex biomarkers detection, Clin. Cancer Res. 15 (2009) 4446–4452.
[9] Z. Wang, N. Liu, F. Feng, Z. Ma, Synthesis of cadmium, lead and copper alginate nanobeads as immunosensing probes for the detection of AFP, CEA and PSA, Biosens. Bioelectron. 70 (2015) 98–105.
[10] J.P. Pursey, Y. Chen, E. Stulz, M.K. Park, P. Kongsuphol, Microfluidic electrochemical multiplex detection of bladder cancer DNA markers, Sens. Actuators B Chem. 251 (2017) 34–39.
[11] M.A. Tainsky, Genomic and proteomic biomarkers for cancer: a multitude of opportunities, Biochim. Biophys. Acta 1796 (2009) 176–193.
[12] R.S. Gomes, F.T.C. Moreira, R. Fernandes, M.G.F. Sales, Sensing CA 15-3 in point-of-care by electropolymerizing *o*-phenylenediamine (OPDA) on Au-screen printed electrodes, PLoS One 13 (2018), e0196656.
[13] H. Fejzić, S. Mujagić, S. Azabagić, M. Burina, Tumor marker CA 15-3 in breast cancer patients, Acta Med. Acad. 44 (2015) 39–46.
[14] J.A. Ribeiro, C.M. Pereira, A.F. Silva, M.G.F. Sales, Disposable electrochemical detection of breast cancer tumour marker CA 15-3 using poly(toluidine blue) as imprinted polymer receptor, Biosens. Bioelectron. 109 (2018) 246–254.
[15] H.Y. Loh, B.P. Norman, K.S. Lai, N.M.A.N.A. Rahman, N.B.M. Alitheen, M. A. Osman, The regulatory role of microRNA in breast cancer, Int. J. Mol. Sci. 20 (2019) 4940.
[16] R. Singh, Y.Y. Mo, Role of microRNAs in breast cancer, Cancer Biol. Ther. 14 (2013) 201–212.
[17] P. Stieber, D. Nagel, I. Blankenburg, V. Heinemann, M. Untch, I. Bauerfeind, D. Di Gioia, Diagnostic efficacy of CA 15-3 and CEA in the early detection of metastatic breast cancer-a retrospective analysis of kinetics on 743 breast cancer patients, Clin. Chim. Acta 448 (2015) 228–231.
[18] E.C. Considine, The search for clinically useful biomarkers of complex disease: a data analysis perspective, Metabolites 9 (2019) 126.
[19] X. Wang, D.R. Walt, Simultaneous detection of small molecules, proteins and microRNAs using single molecule arrays, Chem. Sci. 11 (2020) 7896–7903.
[20] H. Wang, X. Wang, J. Wang, W. Fu, C. Yao, A SPR biosensor based on signal amplification using antibody-QD conjugates for quantitative determination of multiple tumor markers, Sci. Rep. 6 (2016) 33140.
[21] Y. Sun, J. Fan, L. Cui, W. Ke, F. Zheng, Y. Zhao, Fluorometric nanoprobes for simultaneous aptamer-based detection of carcinoembryonic antigen and prostate specific antigen, Microchim. Acta 186 (2019) 152.
[22] B. Babamiri, R. Hallaj, A. Salimi, Ultrasensitive electrochemiluminescence immunoassay for simultaneous determination of CA125 and CA15-3 tumor markers based on PAMAM-sulfanilic acid-Ru(bpy)$_3^{2+}$ and PAMAM-CdTe@CDs nanocomposite, Biosens. Bioelectron. 99 (2018) 353–360.
[23] F. Chen, F. Zhang, Y. Liu, C. Cai, Simply and sensitively simultaneous detection hepatocellular carcinoma markers AFP and miRNA-122 by a label-free resonance light scattering sensor, Talanta 186 (2018) 473–480.
[24] J. Shan, Z. Ma, Simultaneous detection of five biomarkers of lung cancer by electrochemical immunoassay, Microchim. Acta 183 (2016) 2889–2897.
[25] J. Quinchia, D. Echeverri, A.F. Cruz-Pacheco, M.E. Maldonado, J. Orozco, Electrochemical biosensors for determination of colorectal tumor biomarkers, Micromachines 11 (2020) 411.
[26] Z. Ma, N. Liu, Design of immunoprobes for electrochemical multiplexed tumor marker detection, Expert Rev. Mol. Diagn. 15 (2015) 1075–1083.
[27] Z. Tang, Z. Ma, Multiple functional strategies for amplifying sensitivity of amperometric immunoassay for tumor markers: a review, Biosens. Bioelectron. 98 (2017) 100–112.
[28] H.L. Shuai, K.J. Huang, L.L. Xing, Y.X. Chen, Ultrasensitive electrochemical sensing platform for microRNA based on tungsten oxide-graphene composites coupling with catalyzed hairpin assembly target recycling and enzyme signal amplification, Biosens. Bioelectron. 86 (2016) 337–345.
[29] N. Xia, Y. Zhang, X. Wei, Y. Huang, L. Liu, An electrochemical microRNAs biosensor with the signal amplification of alkaline phosphatase and electrochemical–chemical–chemical redox cycling, Anal. Chim. Acta. 878 (2015) 95–101.
[30] D. Feng, L. Li, J. Zhao, Y. Zhang, Simultaneous electrochemical detection of multiple biomarkers using gold nanoparticles decorated multiwall carbon nanotubes as signal enhancers, Anal. Biochem. 482 (2015) 48–54.
[31] F.Y. Kong, B.Y. Xu, J.J. Xu, H.Y. Chen, Simultaneous electrochemical immunoassay using CdS/DNA and PbS/DNA nanochains as labels, Biosens. Bioelectron. 39 (2013) 177–182.
[32] D. Feng, L. Li, X. Han, X. Fang, X. Li, Y. Zhang, Simultaneous electrochemical detection of multiple tumor markers using functionalized graphene nanocomposites as non-enzymatic labels, Sens. Actuators B Chem. 201 (2014) 360–368.
[33] C. Zhu, D. Liu, Y. Li, S. Ma, M. Wang, T. You, Hairpin DNA assisted dual-ratiometric electrochemical aptasensor with high reliability and anti-interference ability for simultaneous detection of aflatoxin B1 and ochratoxin A, Biosens. Bioelectron. 174 (2021), 112654.
[34] X. Chen, Z. Ma, Multiplexed electrochemical immunoassay of biomarkers using chitosan nanocomposites, Biosens. Bioelectron. 55 (2014) 343–349.
[35] X. Chen, X. Jia, J. Han, J. Ma, Z. Ma, Electrochemical immunosensor for simultaneous detection of multiplex cancer biomarkers based on graphene nanocomposites, Biosens. Bioelectron. 50 (2013) 356–361.
[36] X. Zhang, X. Ren, W. Cao, Y. Li, B. Du, Q. Wei, Simultaneous electrochemical immunosensor based on water-soluble polythiophene derivative and functionalized magnetic material, Anal. Chim. Acta 845 (2014) 85–91.
[37] Q. Zhu, Y. Chai, R. Yuan, Y. Zhuo, Simultaneous detection of four biomarkers with one sensing surface based on redox probe tagging strategy, Anal. Chim. Acta 800 (2013) 22–28.

[38] G. Wang, Y. Li, J. Liu, Y. Yuan, Z. Shen, X. Mei, Ultrasensitive multiplexed immunoassay of autophagic biomarkers based on Au/rGO and au nanocages amplifying electrochemcial signal, Sci. Rep. 7 (2017) 2442.
[39] A. Bolotsky, D. Butler, C. Dong, K. Gerace, N.R. Glavin, C. Muratore, J.A. Robinson, A. Ebrahimi, Two-dimensional materials in biosensing and healthcare: from in vitro diagnostics to optogenetics and beyond, ACS Nano 13 (2019) 9781–9810.
[40] J. Narang, A. Mishra, R. Pilloton, A. VV, S. Wadhwa, C.S. Pundir, M. Khanuja, Development of $MoSe_2$ nano-urchins as a sensing platform for a selective bio-capturing of *Escherichia coli* Shiga toxin DNA, Biosensors 8 (2018) 77.
[41] M. Thangamuthu, K.Y. Hsieh, P.V. Kumar, G.Y. Chen, Graphene- and graphene oxide-based nanocomposite platforms for electrochemical biosensing applications, Int. J. Mol. Sci. 20 (2019) 2975.
[42] M. Ahmadi, F. Ahour, An electrochemical biosensor based on a graphene oxide modified pencil graphite electrode for direct detection and discrimination of double-stranded DNA sequences, Anal. Methods 12 (2020) 4541–4550.
[43] M. Pal, R. Khan, Graphene oxide layer decorated gold nanoparticles based immunosensor for the detection of prostate cancer risk factor, Anal. Biochem. 536 (2017) 51–58.
[44] N.N. Song, Y.Z. Wang, X.Y. Yang, H.L. Zong, Y.X. Chen, Z. Ma, C.X. Chen, A novel electrochemical biosensor for the determination of dopamine and ascorbic acid based on graphene oxide/poly(aniline-co-thionine) nanocomposite, J. Electroanal. Chem. 873 (2020), 114352.
[45] N. Wang, J. Wang, X. Zhao, H. Chen, H. Xu, L. Bai, W. Wang, H. Yang, D. Wei, B. Yuan, Highly sensitive electrochemical immunosensor for the simultaneous detection of multiple tumor markers for signal amplification, Talanta 226 (2021), 122133.
[46] S. Chuekachang, R. Janmanee, A. Baba, S. Phanichphant, S. Sriwichai, K. Shinbo, K. Kato, F. Kaneko, N. Fukuda, H. Ushijima, Fabrication of thin film from conducting polymer/single wall carbon nanotube composites for the detection of uric acid, Mol. Cryst. Liq. Cryst. 580 (2013) 1–6.
[47] S. Chuekachang, R. Janmanee, A. Baba, S. Phanichphant, S. Sriwichai, K. Shinbo, K. Kato, F. Kaneko, N. Fukuda, H. Ushijima, Electrochemically controlled detection of adrenaline on poly(2-aminobenzylamine) thin films by surface plasmon resonance spectroscopy and quartz crystal microbalance, Surf. Interface Anal. 45 (2013) 1661–1666.
[48] C. Zhu, G. Yang, H. Li, D. Du, Y. Lin, Electrochemical sensors and biosensors based on nanomaterials and nanostructures, Anal. Chem. 87 (2015) 230–249.
[49] W.S. Hummers, R.E. Offeman, Preparation of graphitic oxide, J. Am. Chem. Soc. 80 (1958) 1339.
[50] T. Krasian, W. Punyodom, P. Worajittiphon, A hybrid of 2D materials (MoS_2 and WS_2) as an effective performance enhancer for poly(lactic acid) fibrous mats in oil adsorption and oil/water separation, Chem. Eng. J. 369 (2019) 563–575.
[51] T. Putnin, W. Jumpathong, R. Laocharoensuk, J. Jakmunee, K. Ounnunkad, A sensitive electrochemical immunosensor based on poly(2-aminobenzylamine) film modified screen-printed carbon electrode for label-free detection of human immunoglobulin G, Artif. Cell. Nanomed. Biotechnol. 46 (2018) 1042–1051.
[52] W. Jumpathong, J. Jakmunee, K. Ounnunkad, A sensitive and disposable graphene oxide electrochemical immunosensor for label-free detection of human immunoglobulin G, Anal. Sci. 32 (2016) 323–328.
[53] P. Norfun, N. Suree, N. Kungwan, W. Punyodom, J. Jakmunee, K. Ounnunkad, Electrochemical detection of human interleukin-15 using a graphene oxide-modified screen-printed carbon electrode, Anal. Lett. 50 (2017) 1112–1125.
[54] S. Chanarsa, J. Jakmunee, K. Ounnunkad, A bifunctional nanosilver-reduced graphene oxide nanocomposite for label-free electrochemical immunosensing, Front. Chem. 9 (2021), 631571.
[55] D. Risović, S. Mahović Poljaček, K. Furić, M. Gojo, Inferring fractal dimension of rough/porous surfaces_A comparison of SEM image analysis and electrochemical impedance spectroscopy methods, Appl. Surf. Sci. 255 (2008) 3063–3070.
[56] R.S. Neves, E. De Robertis, A.J. Motheo, Capacitance dispersion in electrochemical impedance spectroscopy measurements of iodide adsorption on Au(1 1 1), Appl. Surf. Sci. 253 (2006) 1379–1386.
[57] C.H. Kim, S.I. Pyun, J.H. Kim, An investigation of the capacitance dispersion on the fractal carbon electrode with edge and basal orientations, Electrochim. Acta 48 (2003) 3455–3463.
[58] W. Chaocharoen, W. Suginta, W. Limbut, A. Ranok, A. Numnuam, P. Khunkaewla, P. Kanatharana, P. Thavarungkul, A. Schulte, Electrochemical detection of the disease marker human chitinase-3-like protein 1 by matching antibody-modified gold electrodes as label-free immunosensors, Bioelectrochemistry 101 (2015) 106–113.
[59] P. Jolly, M.R. Batistuti, A. Miodek, P. Zhurauski, M. Mulato, M.A. Lindsay, P. Estrela, Highly sensitive dual mode electrochemical platform for microRNA detection, Sci. Rep. 6 (2016) 36719.
[60] R. Tavallaie, J. McCarroll, M. Le Grand, N. Ariotti, W. Schuhmann, E. Bakker, R. D. Tilley, D.B. Hibbert, M. Kavallaris, J.J. Gooding, Nucleic acid hybridization on an electrically reconfigurable network of gold-coated magnetic nanoparticles enables microRNA detection in blood, Nat. Nanotechnol. 13 (2018) 1066–1071.